The intrinsic rate constants in diffusion-influenced reactions

Adithya Vijaykumar,*[ab] Peter G. Bolhuis[b] and Pieter Rein ten Wolde[a]

Intrinsic rate constants play a dominant role in the theory of diffusion-influenced reactions, but usually as abstract quantities that are implicitly assumed to be known. However, recently it has become clear that modeling complex processes requires explicit knowledge of these intrinsic rates. In this paper we provide microscopic expressions for the intrinsic rate constants for association and dissociation processes of isotropically interacting particles and illustrate how these rates can be computed efficiently using rare event simulations techniques. In addition, we address the role of the orientational dynamics, for particles interacting *via* anisotropic potentials.

1 Introduction

The association and dissociation of two particles are elementary steps in many processes in biology, such as receptor–ligand and enzyme–substrate binding in cell signaling, and protein–DNA binding in gene regulation. Also, in materials science association and dissociation play a central role, *e.g.* in the self-assembly of colloidal particles, the formation of micro-emulsions, or the phase behavior of polymer solutions. In these processes, the particles typically come into contact *via* diffusion, after which they bind with a rate that depends on the intrinsic association rate constant; conversely, the associated particles dissociate with an intrinsic dissociation rate, after which they move apart *via* diffusion.

In the past decades, theories of diffusion-influenced reactions have been developed that show how the effective rate constants depend on the diffusion constants of the particles, their cross section, their interaction potential, and the intrinsic association and dissociation rate constants.[1] However, these theories assume, *a priori*, given intrinsic association and dissociation rate constants. Similarly, techniques to simulate networks of chemical reactions have been developed, in which the particles typically have an idealized shape, move by diffusion, and react upon contact with given intrinsic rate constants.[2–7] In parallel, simulation techniques have been developed that enable the calculation of

[a]FOM Institute AMOLF, Science Park 104, 1098 XE Amsterdam, The Netherlands. E-mail: tenwolde@amolf.nl
[b]van't Hoff Institute for Molecular Sciences, University of Amsterdam, PO Box 94157, 1090 GD Amsterdam, The Netherlands. E-mail: p.g.bolhuis@uva.nl
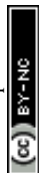
association and dissociation rate constants for pairs of particles that interact *via* potentially complex interaction potentials.[8,9] Yet, these techniques typically compute effective rate constants, which result from the combined effects of diffusion, the interaction potential, and binding upon contact. Moreover, also in experiments typically the effective rate constants are measured. How the intrinsic rate constants depend on the interaction potential, the cross section, and the diffusion constants of the particles, has thus received little attention.

In general, an association–dissociation reaction is a complicated non-Markovian many-body problem that cannot be solved analytically. The reason is that the process of binding generates non-trivial spatio-temporal correlations between the positions of the reactants, which depend on the history of the association and dissociation events. Capturing these correlations requires knowledge of not only the diffusion constants, the interaction potential, and the cross section, but also the intrinsic rate constants.

In dilute systems, however, typically only the effective rate constants are needed to describe the system's dynamics at long times.[10,11] When the concentrations are low, the time it takes for two reactants to meet each other is much longer than the time they spend in close proximity: once the reactants are near each other, they either rapidly bind or rapidly diffuse back into the bulk. Similarly, after a dissociation event, the two reactants either quickly rebind or rapidly move away from each other. Under these conditions, it is often possible to integrate-out the dynamics at the molecular scale, and describe the association–dissociation reaction as a Markovian process with effective association and dissociation rates.[10,11] While these effective rates depend on the intrinsic rate constants, only the effective rate constants determine the dynamics at the relevant length and time scales.[10,11]

Yet, it is now clear that even in dilute systems, spatio-temporal correlations at the molecular scale can dramatically change the behavior of the system at the macroscopic scale.[4,12] In the case of multi-site protein modification, enzyme–substrate rebindings can lead to the loss of ultra-sensitivity and even bi-stability, essentially because rebindings can turn a distributive mechanism into a processive one.[4,12] In such a scenario, even the long-time dynamics cannot be described by effective rate constants: one needs to know the diffusion constants, the cross sections, and the intrinsic rate constants. Moreover, while spatial heterogeneity at the molecular scale can arise from these non-trivial spatio-temporal correlations, in cellular systems microscopic heterogeneity is also imposed *via* molecular structures. In fact, it is now becoming increasingly recognized that cells exploit the spatial heterogeneity of micro-domains, lipid rafts, clusters, and scaffolds as a computational degree of freedom for enhancing information transmission.[13,14] Modeling the reactions in these spatially heterogeneous systems often requires knowledge of the intrinsic rate constants. Last but not least, for simulating association and dissociation reactions in 1D and 2D, knowledge of the intrinsic rate constants is even more pertinent, because no well-defined effective rate constant exists in the long-time limit.

In this manuscript, we provide microscopic expressions for the intrinsic rate constants, and illustrate how these expressions can be used to compute rate constants in rare-event simulation techniques such as Transition Interface Sampling (TIS)[15–17] and Forward Flux Sampling (FFS).[18,19] While computing both the forward and backward rate typically requires two separate simulations, we will

show how, by exploiting analytical expressions for the binding and escape probability, both the association and dissociation rate constants (and hence the equilibrium constant) can be obtained in one single simulation. We discuss the relationship with the technique developed by Northrup and coworkers[8] for computing effective association rates. Finally, we address the role of orientational dynamics in association and dissociation reactions.

2 Theory of diffusion-influenced reactions

We consider two particles A and B that interact *via* an isotropic interaction potential $U(r)$, and move with an interparticle diffusion constant $D = D_A + D_B$, where D_A and D_B are the diffusion constants of A and B, respectively. Upon contact at the interparticle distance σ, the particles can associate with a rate that is determined by the intrinsic associate rate constant k_a, and, when bound, the two can dissociate with an intrinsic dissociation rate k_d. Following the work of Agmon and Szabo,[1] we re-derive in the Appendix the following central results. The effective association rate constant is given by

$$k_{on} = \frac{k_a p_{eq}(\sigma) k_D}{k_a p_{eq}(\sigma) + k_D} = [1 - S_{rad}(t \to \infty | \sigma)] k_D. \tag{1}$$

Here, k_D is the diffusion-limited rate constant, which determines the rate at which the two particles diffuse towards each other, and $p_{eq}(\sigma) \simeq e^{-\beta U(\sigma)}$, with $\beta = 1/(k_B T)$, the inverse temperature, is the equilibrium probability that they are at the distance σ. The survival probability $S_{rad}(t \to \infty | \sigma) = k_D/(k_a p_{eq}(\sigma) + k_D)$ is the probability that the two particles, given that they are at contact, escape into the bulk before binding to each other. Hence, the effective association rate is given by the rate at which the two particles get in contact, which is determined by k_D, and the probability $1 - S_{rad}(t \to \infty | \sigma) = k_a p_{eq}(\sigma)/(k_a p_{eq}(\sigma) + k_D)$ that upon contact, they bind.

The effective dissociation rate is given by

$$k_{off} = \frac{k_d k_D}{k_a p_{eq}(\sigma) + k_D} = k_d S_{rad}(t \to \infty | \sigma). \tag{2}$$

The effective dissociation rate is thus given by the dissociation rate k_d times the probability $S_{rad}(t \to \infty | \sigma) = k_D/(k_a p_{eq}(\sigma) + k_D)$ that the particles upon dissociation diffuse away from each other and escape into the bulk.

It can also be verified that the equilibrium constant is given by

$$K_{eq} = \frac{k_a p_{eq}(\sigma)}{k_d} = \frac{k_{on}}{k_{off}}. \tag{3}$$

At this stage, a few points are worthy of note. First, these results hold for isotropic, but otherwise arbitrary interaction potentials $U(r)$. Secondly, the contact distance σ serves to define the dividing surface that separates the bound from the unbound state. This surface is usually taken to be near the free-energy barrier that separates the bound from the unbound state. The precise location of this dividing surface is somewhat arbitrary, as the effective rate constants cannot by definition depend on the choice made for σ. This is in marked contrast to the intrinsic rate
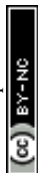
constants k_a and k_d and the diffusion-limited rate k_D, which all sensitively depend on σ. Thirdly, the diffusion-limited rate constant depends not only on σ and D, but also on the interaction potential $U(r)$. For arbitrary interaction potentials $U(r)$, no analytical expression for k_D is, in general, available. However, when σ is chosen to be beyond the range r_c of the interaction potential, then an exact expression is well known—the Smoluchowski diffusion-limited reaction rate constant:[20]

$$k_D = 4\pi\sigma D. \tag{4}$$

Moreover, when $\sigma > r_c$, then $U(\sigma) = 0$, and $p_{eq}(\sigma) = 1$. In this scenario, the effective rate constants are given by:

$$k_{on} = \frac{k_a(\sigma)k_D(\sigma)}{k_a(\sigma) + k_D(\sigma)} \tag{5}$$

$$k_{off} = \frac{k_d(\sigma)k_D(\sigma)}{k_a(\sigma) + k_D(\sigma)}. \tag{6}$$

Here, and below, we have written $k_a = k_a(\sigma)$, $k_d = k_d(\sigma)$ and $k_D = k_D(\sigma)$ to remind ourselves that these rate constants, in contrast to the effective rate constants k_{on} and k_{off}, depend on our choice for σ.

3   Effective positive flux expression

To obtain the intrinsic rate constants in computer simulations, we need expressions in terms of microscopic quantities that can be measured in the simulation. We will focus on the dissociation pathway, and the dissociation rate k_{off}. To compute this rate, we use the "effective positive flux" expression of van Erp and coworkers.[15–17] The progress of the dissociation reaction is quantified via a parameter $\lambda(r)$, which depends on the separation r between the particles A and B. For simplicity, we use $\lambda = r$. A series of interfaces is chosen, $r_0, r_1, \ldots, r_{n-1}, r_n$, such that r_0 is deep in the bound state and r_n is in the unbound state. Strictly speaking the unbound state is defined by $r_n \to \infty$, a point to which we will return in the next section. Defining the history-dependent functions indicator $h_{\mathscr{B}}$ and $h_{\mathscr{U}}$ such that $h_{\mathscr{B}} = 1$ and $h_{\mathscr{U}} = 0$ if the system was more recently in the bound state B ($r < r_0$) than in the unbound state U ($r > r_n$), and $h_{\mathscr{B}} = 0$ and $h_{\mathscr{U}} = 1$ otherwise, the rate constant k_{off} for transitions from B to U is given by[15]

$$k_{off} = \frac{\overline{\Phi_{B,n}}}{\overline{h_{\mathscr{B}}}} = \frac{\overline{\Phi_{B,0}}}{\overline{h_{\mathscr{B}}}} P(r_n|r_0). \tag{7}$$

Here, $\Phi_{B,j}$ is the flux of trajectories coming from the bound state B (with $r < r_0$) that cross r_j for the first time; thus, $\Phi_{B,n}$ is the flux of trajectories from the bound state towards the unbound state, $r > r_n$, and $\Phi_{B,0}$ is the flux reaching the first interface r_0. The factor $\overline{h_{\mathscr{B}}}$ is the average fraction of time that the system spends in the bound state B. $P(r_n|r_0)$ is the probability that a trajectory that reaches r_0 subsequently arrives at interface r_n instead of returning to the bound state r_0. The expression thus states that the total flux of trajectories from the bound state to the unbound state is the flux of trajectories from B to r_0 multiplied by the probability that such a trajectory will later reach r_n before returning to r_0. $P(r_n|r_0)$ can be expressed as the product of the probabilities $P(r_{i+1}|r_i)$ that a trajectory that comes
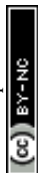
from r_0 and crosses r_i for the first time will subsequently reach r_{i+1} instead of returning to r_0:

$$P(r_n|r_0) = \prod_{i=0}^{n-1} P(r_{i+1}|r_i). \tag{8}$$

Combining eqn (7) and (8), the effective dissociation rate can thus be expressed as

$$k_{off} = \frac{\overline{\Phi}_{B,0}}{\overline{h}_\mathscr{B}} \prod_{i=0}^{n-1} P(r_{i+1}|r_i). \tag{9}$$

The individual factors $P(r_{i+1}|r_i)$ can be determined in a Transition Interface Sampling[15] (TIS) or a Forward Flux Sampling[18,19] (FFS) simulation, as the fraction of trajectories crossing the interface r_i that reach the interface r_{i+1} instead of returning to r_0. FFS and TIS are both based on the effective positive flux expression, eqn (7), but differ in the way they construct the path ensembles.

4   Intrinsic dissociation rate and effective positive flux

To obtain a microscopic expression for the intrinsic dissociation rate k_d, we rewrite eqn (9) as

$$k_{off} = \frac{\overline{\Phi}_{B,0}}{\overline{h}_\mathscr{B}} P(r_{n'}|r_0) P(r_n|r_{n'}), \tag{10}$$

where $P(r'_n|r_0) = \prod_{i=0}^{n'-1} P(r_{i+1}|r_i)$ and $P(r_n|r_{n'}) = \prod_{i=n'}^{n-1} P(r_{i+1}|r_i)$. Now, the crux is to define $r_{n'} \equiv \sigma$. Comparing eqn (10) with eqn (2), we can then make the following identifications:

$$k_d(\sigma) = \frac{\overline{\Phi}_{B,0}}{\overline{h}_\mathscr{B}} P(\sigma|r_0) \tag{11}$$

$$S_{rad}(t \to \infty|\sigma) = \frac{k_D(\sigma)}{k_a p_{eq}(\sigma) + k_D(\sigma)} = P(r_n|\sigma) \tag{12}$$

Eqn (11) provides a microscopic expression for the intrinsic dissociation rate, and is one of the central results of this paper. It shows that the intrinsic dissociation rate is the flux of trajectories that come from the bound state and cross the dividing surface $r_{n'} = \sigma$. The expression makes explicit that the intrinsic dissociation rate depends on the choice for σ. Also eqn (12) highlights the idea that not only the intrinsic rates, but also the diffusion-limited rate k_D depends on this choice. We further iterate that σ need not be chosen beyond the interaction range of the potential; the expressions hold for any choice of σ.

The microscopic expressions of eqn (11) and (12) make it possible to obtain both the effective dissociation rate k_{off} and the intrinsic dissociation rate k_d from computer simulations. Again, transition interface sampling[15] and forward flux
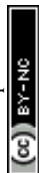
sampling[18,19] are particularly well suited, because they are both based on the effective positive flux expression, eqn (7).

In fact, by choosing the cross-section σ beyond the range r_c of the interaction potential, it is possible to obtain from one simulation not only the intrinsic dissociation rate k_d and effective dissociation rate k_{off}, but also the intrinsic association rate k_a and effective association rate k_{on}, and hence the equilibrium constant K_{eq}. One TIS/FFS simulation yields both k_d, from eqn (11), and $P(r_n|\sigma) = S_{rad}(t \to \infty|\sigma)$, from eqn (12). Yet, when $\sigma > r_c$ (and $U(\sigma) = 0$), we know that the latter is also given by

$$P(r_n|\sigma) = S_{rad}(t \to \infty|\sigma) = \frac{k_D(\sigma)}{k_a(\sigma) + k_D(\sigma)}, \tag{13}$$

with $k_D = 4\pi\sigma D$, as discussed in Section 2. In other words, having computed $P(r_n|\sigma)$ in the TIS/FFS simulation, we can use the above expression and the analytical solution $k_D = 4\pi\sigma D$, to obtain not only k_d but also k_a:

$$k_a(\sigma) = \frac{(1 - P(r_n|\sigma))k_D(\sigma)}{P(r_n|\sigma)}. \tag{14}$$

From k_d and k_a, we obtain the equilibrium constant $K_{eq} = k_a/k_d$, from which we then find $k_{on} = K_{eq}k_{off}$.

As pointed out above, the effective rates are strictly defined for $r_n \to \infty$, meaning that eqn (11) and (14) are also only valid in that limit. However, to keep the simulations tractable, in practice one would like to use an interface at finite r_n. In the next section we derive an expression that holds for finite interface values r_n.

5 Computing the intrinsic rates for an interface at finite r_n

While the intrinsic association rate constant k_d does not rely on taking the position of the last interface $r_n \to \infty$, the intrinsic rate constant k_a does (see eqn (14)). To obtain an expression for k_a for a finite value of r_n, we start by rewriting the effective association rate eqn (6) as the sum of reciprocal intrinsic rates:

$$\frac{1}{k_{on}} = \frac{1}{k_a(\sigma)} + \frac{1}{k_D(\sigma)}. \tag{15}$$

Since the effective association rates are independent on the choice of the dividing surface σ, we can choose to set the dividing surface at $r_n > \sigma$

$$\frac{1}{k_{on}} = \frac{1}{k_a(r_n)} + \frac{1}{k_D(r_n)}. \tag{16}$$

Combining the above two equations and rearranging yields

$$\frac{1}{k_a(r_n)} - \frac{1}{k_a(\sigma)} = \frac{1}{k_D(\sigma)} - \frac{1}{k_D(r_n)}. \tag{17}$$

To make progress we need to relate the intrinsic rate constants $k_a(\sigma)$ and $k_a(r_n)$. This relation is provided by linking the intrinsic dissociation rates, eqn (11) at the respective surfaces, yielding

$$k_d(r_n) = \frac{\overline{\Phi_{B,0}}}{\overline{h_{\mathscr{B}}}} P(r_n|r_0) = \frac{\overline{\Phi_{B,0}}}{\overline{h_{\mathscr{B}}}} P(\sigma|r_0)P(r_n|\sigma) = k_d(\sigma)P(r_n|\sigma). \tag{18}$$

Since detailed balance implies $K_{eq} = k_a(\sigma)/k_d(\sigma) = k_a(r_n)/k_d(r_n)$, the desired relation for the intrinsic association rate constants is

$$k_a(r_n) = k_a(\sigma)P(r_n|\sigma). \tag{19}$$

Inserting eqn (19) into eqn (17) and rearranging yields

$$k_a(\sigma) = \frac{(1 - P(r_n|\sigma))k_D(\sigma)}{P(r_n|\sigma)(1 - \Omega)}, \tag{20}$$

where $\Omega \equiv k_D(\sigma)/k_D(r_n)$ which, using $k_D(b) = 4\pi\sigma b$, reduces to $\Omega = \sigma/r_n$. Eqn (20) provides an explicit expression for the intrinsic association rate k_a for finite r_n, featuring a correction factor $1/(1 - \Omega)$. For $r_n \rightarrow \infty$, Ω vanishes and the expression reduces to eqn (14). However, the correction factor decays slowly with r_n, and in practice it cannot be neglected. Since Ω is known analytically, eqn (20) turns this approach into a feasible strategy for computing both k_d and k_a in TIS and FFS, which directly give access to $P(r_n|\sigma)$. Lastly, combining this expression with eqn (5) and (6), we obtain the following expressions for the effective on and off rates, respectively:

$$k_{on} = \frac{(1 - P(r_n|\sigma))k_D(\sigma)}{1 - P(r_n|\sigma)\Omega}, \tag{21}$$

$$k_{off} = k_d(\sigma)P(r_n|\sigma)\frac{1 - \Omega}{1 - P(r_n|\sigma)\Omega}. \tag{22}$$

5.1 Illustrative example

As an illustration of the above scheme we numerically evaluated eqn (20) for a two particle system undergoing Brownian dynamics (BD).[22] The interaction potential between the two particles is given by

$$U(r) = \begin{cases} 4\varepsilon\left[\left(\frac{\sigma_{LJ}}{r}\right)^{12} - \left(\frac{\sigma_{LJ}}{r}\right)^{6}\right], & 0 < r < 3\sigma_{LJ} \\ 0, & r > 3\sigma_{LJ} \end{cases}, \tag{23}$$

where σ_{LJ} sets the length-scale of the Lennard–Jones potential, ε sets the well depth, and r is the interparticle distance. In the simulations $\sigma_{LJ} = 5$ nm, $\varepsilon = 10k_BT$. The length of the simulation box is $60\sigma_{LJ}$. We evaluate $k_d(\sigma)$ and $P(r_n|\sigma)$ using one single FFS simulation. First, we fix the cross section $\sigma = 3\sigma_{LJ}$, just beyond the cut-off distance of the potential. Interfaces were set at $r = \{1.3, 1.5, 2.0, 2.5, 3.0, 3.2, 3.4, 3.6, 3.8, 4.0, 4.2, 4.4, 4.6, 4.8, 5.0, 5.5, 6.0, 6.5\}$, in units of σ_{LJ}. From each interface, 10 000 trajectories are started and the conditional probability as in eqn (8) is calculated.

We test the independence of eqn (20) on the location of the final interface by varying r_n, while keeping $\sigma = 3.0\sigma_{LJ}$ fixed. As seen in Fig. 1 (left) the value of $k_a(\sigma)$ is
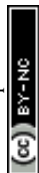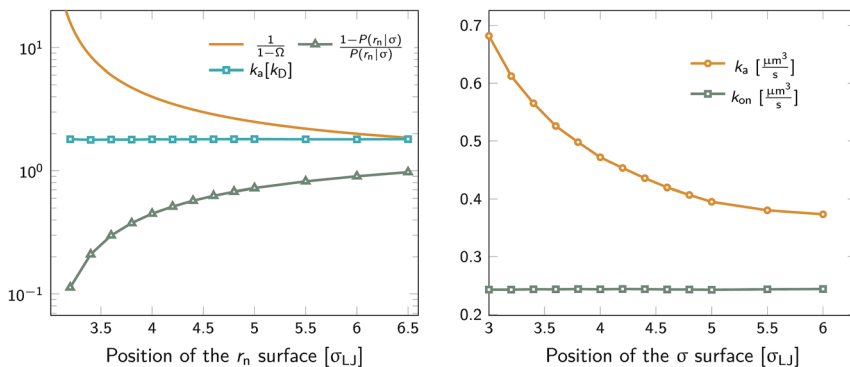
Fig. 1 The intrinsic rate constant for the isotropic Lennard–Jones potential. Left: $k_a(\sigma)$ as a function of the position of last interface, r_n in units of $k_D(\sigma)$, for a fixed cross section $\sigma = 3\sigma_{LJ}$. The correction factor $\dfrac{1}{1-\Omega}$ and the factor $(1 - P(r_n|\sigma))/P(r_n|\sigma)$ are also shown. As expected, the value of $k_a(\sigma)$ remains constant as r_n is varied. Right: $k_a(\sigma)$ and k_{on} as a function of the cross section σ. The position of the last interface, r_n, is kept constant at $6.5\sigma_{LJ}$. It is seen that while k_a varies with σ, k_{on} does not.

independent of the position of the r_n surface. Note, however, that the correction factor $1/(1 - \Omega)$ is not negligible, even for $r_n = 6.5\sigma_{LJ}$.

Next, we plot in Fig. 1 (right) the dependence of the intrinsic association rate $k_a(\sigma)$ on the location of the cross section σ, keeping $r_n = 6.5\sigma_{LJ}$ constant. The intrinsic association rate constant decreases with σ, but the effective rate constant k_{on} is independent of σ, as expected.

The intrinsic dissociation rate $k_d(\sigma)$ is evaluated *via* eqn (11). From $k_d(\sigma)$ and $k_a(\sigma)$, the values of k_{on} and k_{off}, are evaluated using eqn (5) and (6). K_{eq} is calculated using eqn (3). The results are summarized in Table 1.

5.2 Validation of the effective rate constants

To validate the values of k_{on} and k_{off} obtained from the FFS simulations, we calculate these values also from a brute force Brownian dynamics simulation of the same system of two particles. First, the equilibrium constant K_{eq} is evaluated using the analytic expression

$$K_{eq} = 4\pi \int_0^{3\sigma_{LJ}} r^2 e^{-\beta U(r)} \mathrm{d}r = \frac{k_{on}}{k_{off}}, \tag{24}$$

where $U(r)$ is given by eqn (23), and the integral is over the bound state $0 < r < 3\sigma_{LJ}$.

Table 1 Comparison of the effective rate constants as determined *via* different approaches: FFS, using eqn (3) and (18)–(22); the autocorrelation function, eqn (25) and (26); the power spectrum, eqn (27). The Table shows good agreement between the values of k_{on} and k_{off}, and hence K_{eq}, obtained *via* these different approaches

	$K_{eq}/10^{-3}\ \mu m^3$	$k_{on}/\mu m^3\ s^{-1}$	k_{off}/s^{-1}
FFS	5.127	0.2417	47.14
Time autocorrelation	5.145	0.2589	50.33
Power spectrum	5.145	0.2571	49.99
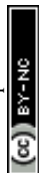
The brute force simulation generates a time trace $n(t)$, switching from the bound state with $n(t) = 1$ to the unbound state with $n(t) = 0$. From this time trace we generate a time autocorrelation function

$$c(\tau) = \frac{\langle n(\tau)n(0)\rangle}{\langle n(0)^2\rangle} \approx e^{-\mu\tau}, \tag{25}$$

that relaxes exponentially with a decay constant μ given by

$$\mu = k_{on}/V + k_{off}. \tag{26}$$

Fig. 2 shows this time autocorrelation function. The simulation results are fitted to eqn (25) to obtain the value of μ and by combining with eqn (24) and (26), the effective rate constants are obtained.

Alternatively, we can generate a power spectrum $P(\omega)$ from the same $n(t)$ time trace.[10] The power spectrum for a random telegraph process with switching rates k_f and k_b is given by

$$P(\omega) = \frac{2\mu p(1-p)}{\mu^2 + \omega^2}, \tag{27}$$

where ω is the frequency, $\mu = k_f + k_b$ is the decay rate and $p = k_f/(k_f + k_b)$. The low-frequency part of the power spectrum as obtained from the simulations is expected to be given by the above expression, with $k_f = k_{on}/V$ and $k_b = k_{off}$ (see ref. 10). Table 1 compares the values of k_{on} and k_{off} as obtained via this scheme, with those from FFS, using eqn (3) and (18–22), and the results from the time autocorrelation function, eqn (25) and (26). It is seen that the values are in very good agreement.

6 Relation to other techniques

Northrup et al.[8,21] provide a method to compute the effective association rate directly from eqn (1)

$$k_{on} = [1 - S_{rad}(t \to \infty|\sigma)]k_D(\sigma) \equiv \beta_\infty k_D(\sigma), \tag{28}$$

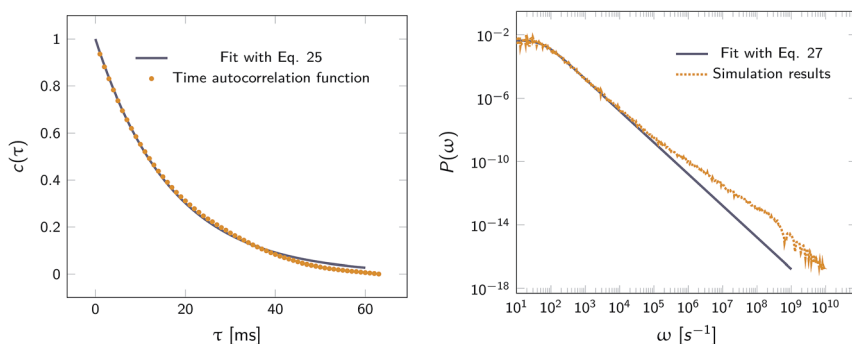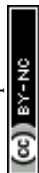
Fig. 2 Left: The autocorrelation function $c(\tau)$ obtained from simulation is fit to eqn (25), yielding $\mu = 59.9236$ s^{-1}. Right: Power spectrum $P(\omega)$ fitted to eqn (27) to determine the value of $\mu = 59.5192$ s^{-1}. In both cases the effective rate constants are calculated by solving eqn (26) and (24).

where $\beta_\infty = 1 - S_{rad}(t \to \infty | \sigma)$ is defined as the probability that particles starting at a distance σ associate rather than diffuse away and escape into the bulk. This probability can be computed explicitly by generating trajectories from an isotropically distributed ensemble of configurations of particles at distance σ. To prevent needlessly long trajectories, Northrup et al. introduced an additional surface c at which they halt the trajectories. The computed association probability $\beta \neq \beta_\infty$ is now defined as the chance to associate rather than to escape to c. They then relate β to β_∞ using a branching method, adding up all probabilities of paths that leave c but return to σ rather than reach infinity,[21] yielding a geometric series that can be written as

$$\beta_\infty = \frac{\beta}{1 - (1 - \beta)\Omega}, \tag{29}$$

where $\Omega = k_D(\sigma)/k_D(c) = \sigma/c$. As the association probability β_∞ is related to the intrinsic rate constant through $\beta_\infty = k_a(\sigma)/(k_a(\sigma) + k_D(\sigma))$, it follows that

$$k_a(\sigma) = \frac{\beta k_D(\sigma)}{(1 - \beta)(1 - \Omega)}. \tag{30}$$

The link with the intrinsic rate constant expression eqn (20) can be made by realizing that the association probability $\beta = 1 - P(c|\sigma)$, leading to

$$k_a(\sigma) = \frac{(1 - P(c|\sigma))k_D(\sigma)}{P(c|\sigma)(1 - \Omega)}. \tag{31}$$

This expression is identical to eqn (20), with $c = r_n$. Strikingly, while derived in a different way, the intrinsic rate expression based on the Northrup method yields the same correction factor as our analysis for finite interfaces.

7 Anisotropic interactions

The above derivations hold for particles interacting via an isotropic pair potential. However, many molecular systems, such as proteins and ligands, have anisotropic interactions that depend on the relative orientation of the particles. For such systems it is not immediately clear whether the expressions derived above are still valid. The point is that while the Boltzmann distribution of the particles' orientations is isotropic beyond the cutoff distance of the potential, the distribution in the ensemble of reactive trajectories, as harvested by TIS and FFS, is not: in these reactive trajectories, the particles tend to have their patches aligned. Naturally, one can still define and measure an effective association and dissociation rate. Yet, the simple expressions derived in the Appendix are no longer valid.

Following Northrup et al.,[8,21] one can always express the effective association rate for anisotropic particles as

$$k_{on} = \beta_\infty k_D(\sigma), \tag{32}$$

where the diffusion-limited rate constant is again $k_D(\sigma) = 4\pi D\sigma$, and β_∞ is given by eqn (29). Now, we define the intrinsic rate $k_a(\sigma)$ via $\beta_\infty \equiv k_a(\sigma)/(k_a(\sigma) + k_D(\sigma))$, which yields
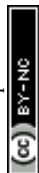
$$k_a(\sigma) = \frac{\beta k_D(\sigma)}{(1 - \beta)(1 - \Omega)}, \tag{33}$$

with Ω, as before, given by $\Omega = k_D(\sigma)/k_D(c)$. This yields an explicit expression for $k_a(\sigma)$ in terms of the probability β of binding rather than reaching the surface $r_n = c$, starting from an isotropic distribution at the surface σ; this is indeed the essence of the technique of Northrup et al.[21] When the distribution, as generated in the TIS/FFS simulation, is isotropic at σ then eqn (20) and (33) with $\beta = 1 - P(r_n|\sigma)$ are equivalent and both can be used. The problem arises when we want to connect eqn (33) to the expression used in TIS/FFS to compute the dissociation rate in the case that the distribution at σ is not isotropic. The principal idea of the scheme presented in Sections 4 and 5 is that $P(r_n|\sigma)$, as obtained in a TIS/FFS computation of the dissociation rate, is given by the analytical result $k_D(\sigma)/(k_a(\sigma) + k_D)$, for $r_n \to \infty$. We could thus use this analytical result to obtain the intrinsic rate $k_a(\sigma)$ in eqn (13) and (14); the expression that relates $P(r_n|\sigma)$ to $k_a(\sigma)$ when r_n is finite, is eqn (20). However, in the case of anisotropic interaction potentials the distribution of reactive trajectories at the σ interface can also become anisotropic. In that case one can no longer identify $P(r_n|\sigma)$ as obtained in an TIS/FFS simulation with $1 - \beta$ in eqn (33), and (20) or (33) cannot be used to obtain $k_a(\sigma)$ from a TIS/FFS simulation. In summary, when the distribution at σ as obtained in the TIS/FFS simulation is isotropic, we expect both eqn (33) and (20) to hold. However, if the distribution is not isotropic eqn (20) ceases to be valid.

Nevertheless, even when the potential is anisotropic, eqn (20) still provides a route towards computing $k_a(\sigma)$. Indeed if, at a certain interface σ' sufficiently far away from contact, the distribution of trajectories has become uniform the intrinsic rate for that surface is given by eqn (20)

$$k_a(\sigma') = \frac{(1 - P(r_n|\sigma'))k_D(\sigma')}{P(r_n|\sigma')(1 - \Omega)}, \tag{34}$$

where $\Omega = k_D(\sigma')/k_D(r_n)$, and $r_n > \sigma'$. Since we know that the effective association rate is independent of the choice of the dividing surface, we can write

$$\frac{1}{k_{on}} = \frac{1}{k_a(\sigma)} + \frac{1}{k_D(\sigma)} = \frac{1}{k_a(\sigma')} + \frac{1}{k_D(\sigma')}, \tag{35}$$
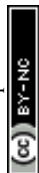
even if the distribution at σ is anisotropic. Inserting eqn (34) into this identity gives

$$\frac{1}{k_a(\sigma)} = \frac{P(r_n|\sigma')(1 - \Omega)}{(1 - P(r_n|\sigma'))k_D(\sigma')} + \frac{1}{k_D(\sigma')} - \frac{1}{k_D(\sigma)}, \tag{36}$$

or, rearranging,

$$k_a(\sigma) = \frac{(1 - P(r_n|\sigma'))k_D(\sigma')k_D(\sigma)}{P(r_n|\sigma')(k_D(\sigma') - k_D(\sigma)\Omega) + k_D(\sigma) - k_D(\sigma')}. \tag{37}$$

This expression reduces to eqn (20) when $\sigma = \sigma'$, as expected. For $\sigma \neq \sigma'$, the expression holds even when the distribution at σ is anisotropic, provided that the distribution at σ' is isotropic. The value of $k_a(\sigma)$ thus obtained *via* a TIS/FFS

computation of the dissociation pathway, yielding an anisotropic distribution at σ, is the same as that would have been obtained from a simulation of the association pathway *via* the Northrup scheme starting from a uniform distribution at σ.

Inserting eqn (36) into (35) yields

$$k_{\text{on}} = \frac{(1 - P(r_n|\sigma'))k_{\text{D}}(\sigma')}{1 - \Omega P(r_n|\sigma')}, \tag{38}$$

which is indeed identical to eqn (21) with $\sigma = \sigma'$. Since k_{on} is independent of the interface σ', the rate given by eqn (38) as a function of σ' should reach a constant value. Any deviation from this limiting value is due to a loss of isotropy. Hence, this expression provides a criterion for testing the isotropy requirement.

7.1 Illustrative example

We consider a system comprising two patchy particles interacting *via* a pair potential that consists of several contributions. The particles interact *via* a center–center potential $V_{\text{cc}}(r) = V_{\text{cc-rep}}(r) + V_{\text{cc-att}}(r)$ based on the distance r between the centers of mass, that is in turn built up from a repulsive and an attractive potential. Additionally, there is an attractive patch–patch pair interaction $V_{\text{pp}}(\delta)$ based on the distance δ between two points (patches) located on either particle's surface. Fig. 3 illustrates this setup. The total pair interaction potential is thus

$$V(r,\delta) = V_{\text{cc-rep}}(r) + V_{\text{cc-att}}(r) + V_{\text{pp}}(\delta). \tag{39}$$

Note that δ implicitly depends on the location of the patch, and hence on the orientation of the particle. The potential $V_{\text{cc-rep}}(r)$, $V_{\text{cc-att}}(r)$ and $V_{\text{pp}}(\delta)$ have the simple quadratic form

$$V_i(x) = \begin{cases} \varepsilon_i\left(1 - a_i\left(\dfrac{x}{d}\right)^2\right) & \text{if } x < x_i^*, \\[2mm] \varepsilon_i b_i\left(\dfrac{x_i^c}{d} - \dfrac{x}{d}\right)^2 & \text{if } x_i^* < x < x_i^c, \\[2mm] 0 & \text{otherwise.} \end{cases} \tag{40}$$

where the index i refers to one of the labels {cc-rep, cc-att, pp}, and d is the particle diameter and sets the length scale. The overall strength ε_i, the stiffness a_i and the parameter x_i^*, which combined with a_i determines the range of the potential, are free parameters. Cut-offs x_i^c and smoothing parameters b_i are fixed by requiring continuity and differentiability at x_i^*. These potentials give us a firm control over the potential shape, and allow for easy integration with potentials that are short-ranged and highly orientation-specific. For our illustrative purposes, we take the following parameters: $\varepsilon_{\text{cc-rep}} = 100k_{\text{B}}T$, $a_{\text{cc-rep}} = 1$ and $R_{\text{cc-rep}}^* = 0.85d$, implying $b_{\text{cc-rep}} = 2.6036$ and $R_{\text{cc-rep}}^c = 1.1764d$; $\varepsilon_{\text{pp}} = 20k_{\text{B}}T$, $a_{\text{pp}} = 20$ and $r_{\text{pp}}^* = 0.1d$, implying $b_{\text{pp}} = 5$ and $r_{\text{pp}}^c = 0.5d$; and $\varepsilon_{\text{cc-att}} = 10k_{\text{B}}T$, $a_{\text{cc-att}} = 1$ and $R_{\text{cc-att}}^* = 0.85d$, implying $b_{\text{cc-rep}} = 2.6036$ and $R_{\text{cc-rep}}^c = 1.1764d$.
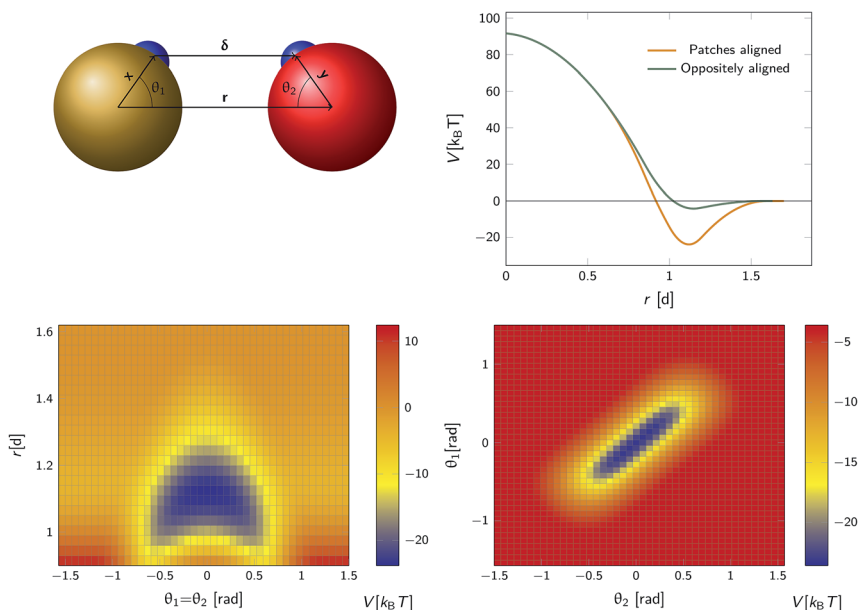
Fig. 3 The anisotropic interaction potential. Top left: The particles interact *via* a combination of a center–center potential $V_{cc}(r)$ and a patch–patch attraction $V_{pp}(\delta)$ between the small patches on the surface of the particle. Top right: Total interaction potential $V_{cc}(r) + V_{pp}(r - d)$ for two particles with perfectly aligned complementary patches (orange solid curve), and oppositely aligned patches $V_{cc}(r) + V_{pp}(r + d)$ (dark green curve). The existence of patches introduces a strongly attractive bound state with the aligned particles in close contact. Bottom left: Heat map of the potential as a function of the distance between centres of mass r and the angle between the patch vector and inter-particle vector, θ_1 and θ_2 (see also top left) with $\theta_1 = \theta_2$. Bottom right: Heat map of potential as a function of θ_1, θ_2 given $r = 1.1d$. Note the relatively narrow range of orientations over which strong bonding occurs.

As an illustration we plot in Fig. 3 the total inter-particle potential as a function of r when the two complementary patches are aligned to face each other, so that $\delta = r - d$. A narrow attractive well arises when the two particles are in close contact. In the same plot we also give the inter-particle potential as a function of r when the two complementary patches are oppositely aligned (with the patches facing in opposite directions) so that $\delta = r + d$. Here, there is only a very shallow attractive interaction at contact, caused by the isotropic center–center potential $V_{cc}(r)$. In Fig. 3 we also demonstrate the orientational dependence of the attractive potential, showing that the attractive interaction is highly sensitive to misalignment.

A Brownian dynamics (BD) simulation employing an anisotropic potential requires translation as well rotational dynamics. We use a first order quasi-symplectic BD integrator which works particularly well for orientational dynamics,[23] and can be straightforwardly combined with FFS. We performed an FFS simulation, with interfaces based on the binding energy when the particles are within the range of the potential,[23] and beyond that with interfaces based on the center-to-center distance r: $r = \{1.5, 1.6, 1.8, 2.0, 2.2, 2.4, 2.6, 2.8, 3.0, 3.5, 5.5, 6.5, 7.5\}$ in
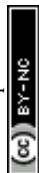
units of d. From each interface, 10 000 trajectories are started, and the conditional probability as in eqn (8) is calculated.

To illustrate that eqn (20) does not hold when the distribution at σ is not isotropic, we evaluated $k_a(\sigma)$ using this equation for a fixed cross section $\sigma = 1.5d$, see Fig. 4. The range of the anisotropic interaction potential depends on the orientation, but even when the patches are aligned (and the range is maximal), the potential approaches zero beyond $1.5d$ (see Fig. 3); this is indeed why we have chosen the cross-section to be $\sigma = 1.5d$. Fig. 4 shows $k_a(\sigma)$ as a function of the position of the last interface, r_n. It also shows the factors $1/(1 - \Omega) = 1/(1 - \sigma'/r_n)$ and $1 - P(r_n|\sigma')/P(r_n|\sigma')$, which both depend on r_n. However, while for the isotropic potential, $k_a(\sigma)$ is independent of r_n as long as σ (and r_n) are beyond the range of the interaction potential (see Fig. 1), here this is not the case, because the distribution at σ is not isotropic. This shows that eqn (20) cannot be used for anisotropic interactions, if at σ the orientational distribution of the particles is still anisotropic.

However, plotting the effective rate k_{on} given by eqn (38) as a function of σ' for $r_n = 7.5d$ in Fig. 5 (left), shows that k_{on} becomes constant beyond $\sigma' = 3d$, indicating that this is the distance at which the particles become isotropically distributed. This observation allows us, via eqn (37), to determine $k_a(\sigma)$, even when at σ the distribution is not isotropic. This is illustrated in Fig. 5 (right), which shows $k_a(\sigma)$ as a function of σ from eqn (37), for several values of σ', and for a fixed position of the last interface, $r_n = 7.5d$. The intrinsic rate shows qualitatively similar behavior as in Fig. 1, but for $\sigma' < 3d$, the value of $k_a(\sigma)$ does depend on σ', because the distribution at σ' is not isotropic yet. However, for $\sigma' > 3d$, $k_a(\sigma)$ becomes independent of σ', and the intrinsic rate constant k_a can thus be obtained for all values of σ that are beyond the range of the interaction potential.
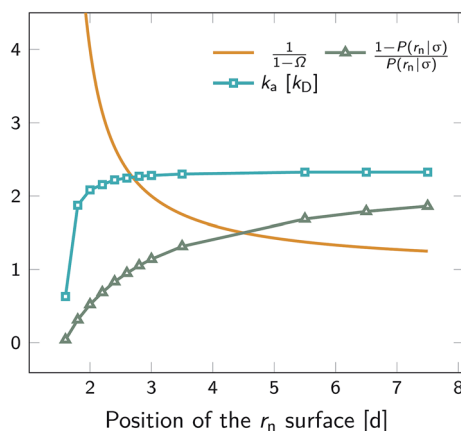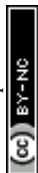

Fig. 4 The intrinsic rate constant $k_a(\sigma)$ from eqn (20) (in units of $k_D(\sigma)$) as a function of the position of the last interface, r_n, for the anisotropic interaction potential shown in Fig. 3. The cross section σ surface is kept constant at $1.5d$. The correction factor $1/(1 - \Omega) = 1/(1 - \sigma'/r_n)$ and the factor $(1 - P(r_n|\sigma'))/P(r_n|\sigma')$ are also shown. In contrast to the behavior for the isotropic potential, Fig. 1, the value of $k_a(\sigma)$ depends on r_n, even when r_n is beyond the range of the potential $r > \sigma = 1.5d$. This is because for this anisotropic potential the distribution at σ is not uniform. As a result, eqn (20) cannot be used.
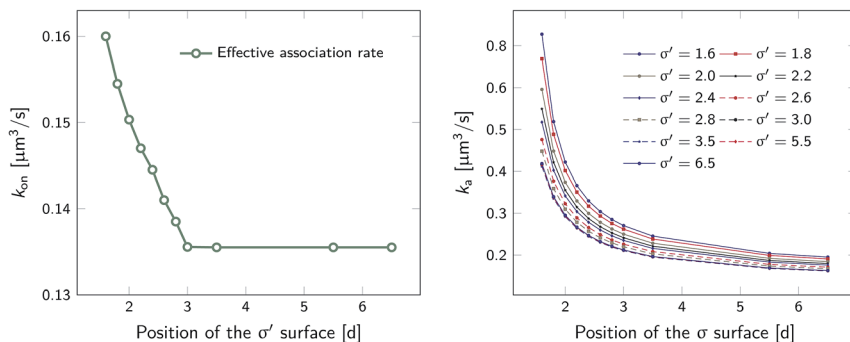
Fig. 5 The effective and intrinsic association rates for the anisotropic potential of Fig. 3. Left: Effective association rate k_{on}, computed *via* eqn (38), as a function of the position of the σ' surface, with the position of the last surface fixed at $r_n = 7.5d$. The value of k_{on} is constant for $\sigma' \geq 3d$, indicating that at and beyond this surface the particles are isotropically distributed. Right: The intrinsic rate constant $k_a(\sigma)$, computed *via* eqn (37), as a function of the cross section σ for different positions of the σ' surface, with the position of the last interface fixed at $r_n = 7.5d$. The curves for $\sigma' = 3.0, 3.5, 5.5, 6.5$ overlap since the distribution of particles beyond this distance has become isotropic. For these values of σ', $k_a(\sigma)$ as a function of σ can be obtained.

8   Conclusion

In this work we derived explicit microscopic expressions for the intrinsic rate constants for diffusion influenced reactions. Remarkably all intrinsic and effective rate constants, as well as the equilibrium constant can be computed from a single TIS or FFS simulation of the dissociation process. To the best of our knowledge this is a new result, and has not been reported in the literature before. We illustrated that this approach works for generic isotropic potentials and even for anisotropic potentials when the reference interface is sufficiently far from contact such that the orientational distributions are isotropic. This later condition led to a criterion for testing this isotropic behavior.

The results obtained in this paper are very general and can be used to compute accurate rate constants in complex systems using rare events techniques such as forward flux sampling or transition interface sampling. In future work we will also study how the magnitude of the intrinsic rate constant compares to that of the diffusion-limited rate constant, and how this depends on the binding affinity. This question is, for instance, important for understanding how tightly diffusion puts a fundamental upper bound on the precision of chemical sensing.[11,24–26]

Appendix A

The rate constants for two particles that interact *via* an isotropic interaction potential

It will be instructive to first revisit the derivation of the rate constants. Following Agmon and Szabo,[1] we consider a single static receptor at the origin and a single ligand molecule that moves with diffusion constant D. The probability that the ligand molecule is at distance r at time t given that it was initially at a distance r_0 is

Faraday Discussions
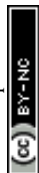
given by the Green's function $P(r,t|r_0)$. The evolution of the Green's function is given by the diffusion equation

$$\frac{\partial p(r,t|r_0)}{\partial t} = \frac{1}{r^2}\frac{\partial}{\partial r}Dr^2e^{-\beta U(r)}\frac{\partial}{\partial r}e^{\beta U(r)}p(r,t|r_0),\qquad(41)$$

where β is the inverse temperature and $U(r)$ is the interaction potential. The effective association and dissociation rate constants are obtained by solving eqn (41) with different boundary conditions. We start with the association reaction.

Association reaction

To obtain the effective association rate constant k_{on}, we solve eqn (41) subject to the boundary condition

$$4\pi\sigma^2 D\frac{\partial p(r,t|r_0)}{\partial r}\bigg|_{r=\sigma} = k_a p(\sigma,t|r_0).\qquad(42)$$

Here k_a is the intrinsic rate constant, which determines the rate at which receptor and ligand associate given they are at the contact distance σ. If k_a is finite, then the boundary condition is called a radiation boundary condition, while if $k_a \to \infty$, the boundary condition is an absorbing condition. The latter can be used to obtain the rate constant of diffusion-limited reactions, where receptor and ligand associate upon the first collision.

The survival probability $S_\alpha(t|r_0)$ is the probability that a particle, which starts at a position r_0, has not yet reacted at a later time t. It is given by

$$S_\alpha(t|r_0) = 4\pi\int_\sigma^\infty \mathrm{d}r r^2 p(r,t|r_0).\qquad(43)$$

The subscript α is either "rad" or "abs", corresponding to k_a being finite or infinite, respectively. The propensity function $R_\alpha(t|r_0)$ is the probability that a ligand particle, which starts at $r = r_0$, reacts for the first time at a later time t:

$$R_\alpha(t|r_0) = -\frac{\partial S_\alpha(t|r_0)}{\partial t}.\qquad(44)$$

The time-dependent rate constant $k_\alpha(t)$ is

$$k_\alpha(t) = 4\pi\int_\sigma^\infty \mathrm{d}r_0 r_0^2 R_\alpha(t|r_0)p_{eq}(r_0).\qquad(45)$$

The distribution $p_{eq}(r_0)$ is the equilibrium radial distribution function, $p_{eq}(r) = e^{-\beta U(r)}$. If ligand and receptor only interact at contact, then $U(r) = 0$ for $r \geq \sigma$ and $p_{eq} = 1$, meaning that the equilibrium distribution corresponds to a spatially uniform distribution. The time-dependent rate constant $k_\alpha(t)$ divided by the volume V is the probability per unit amount of time that receptor and ligand associate for the first time at a later time t, averaged over all initial positions r_0 drawn from the equilibrium distribution $p_{eq}(r_0)$.

The expressions eqn (43)–(45) hold for both radiating and absorbing boundary conditions, corresponding to k_a being finite and infinite, respectively. When k_a is finite, $R_{rad}(t|r_0)$ is also given by

$$R_{rad}(t|r_0) = k_a p(\sigma, t|r_0) \tag{46}$$

and the time-dependent rate constant $k_{rad}(t)$ is then also given by

$$k_{rad}(t) = 4\pi k_a \int_\sigma^\infty dr_0 r_0^2 p(\sigma, t|r_0) p_{eq}(r_0) \tag{47}$$

To relate $k_{rad}(t)$ to $k_{abs}(t)$ in what follows below it will be useful to exploit the detailed-balance condition

$$p_{eq}(r_0) p(r, t|r_0) = p_{eq}(r) p(r_0, t|r). \tag{48}$$

We can integrate this equation over r_0 to find

$$4\pi \int dr_0 r_0^2 p(r, t|r_0) p_{eq}(r_0) = p_{eq}(r) S_\alpha(t|r). \tag{49}$$

Combining this equation with eqn (47) we find that

$$k_{rad}(t) = p_{eq}(\sigma) k_a S_{rad}(t|\sigma). \tag{50}$$

The time-dependent rate constant $k_{rad}(t)$ can be related to the time-dependent rate constant $k_{abs}(t)$ *via*

$$k_{rad}(t) = \int_0^t dt' R_{rad}\left(t - t'\middle|\sigma\right) k_{abs}(t'). \tag{51}$$

This can be understood by noting that $k_{abs}(t')/V$ is the probability per unit amount of time that receptor and ligand come in contact for the first time at time t', while $R_{rad}(t - t')|\sigma$ is the probability that receptor and ligand which start at contact $r = \sigma$ at time t' associate a time $t - t'$ later. In Laplace space, the above expression reads

$$\hat{k}_{rad}(s) = \hat{R}_{rad}(s|\sigma) \hat{k}_{abs}(s). \tag{52}$$
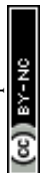
Since $R_{rad}(t|\sigma) = -\partial S_{rad}(t|\sigma)/\partial t$, $\hat{R}_{rad}(s|\sigma)$ is also given by

$$\hat{R}_{rad}(s|\sigma) = 1 - s\hat{S}_{rad}(s|\sigma). \tag{53}$$

Combining the Laplace transform of eqn (50) with eqn (52) and (53) yields

$$\hat{k}_{rad}(s) = \frac{k_a p_{eq}(\sigma) \hat{k}_{abs}(s)}{k_a p_{eq}(\sigma) + s\hat{k}_{abs}(s)}. \tag{54}$$

The effective association rate k_{on} is given by the long-time limit of $k_{rad}(t)$. Using eqn (54) we thus find:

$$k_{on} = \lim_{t \to \infty} k_{rad}(t) = \lim_{s \to 0} s\hat{k}_{rad}(s) = \frac{k_a p_{eq}(\sigma)k_D}{k_a p_{eq}(\sigma) + k_D}. \tag{55}$$

Here, $k_D = \lim_{s \to 0} s\hat{k}_{abs}(s)$ is the diffusion-limited association rate for two particles interacting *via* an interaction potential $U(r)$. By combining eqn (50) with eqn (52) and (53), it also follows that the probability that a particle at contact σ does not bind but escapes, is

$$S_{rad}(\infty|\sigma) = \lim_{s \to 0} s\hat{S}(s|\sigma) = \frac{k_D}{k_a p_{eq}(\sigma) + k_D}. \tag{56}$$

Hence, the effective association rate constant, eqn (55), can be interpreted as being given by the rate constant k_D of arriving at the surface σ, followed by the probability $1 - S_{rad}(\infty|\sigma) = k_a p_{eq}(\sigma)/(k_a p_{eq}(\sigma) + k_D)$ that the arrival leads to binding.

The results derived above hold for arbitrary $p_{eq}(r) = e^{-\beta U(r)}$. We now consider the case that $U(r) = 0$ for $r \geq \sigma$. The time-dependent rate constant $k_{abs}(t)$ is then[27]

$$k_{abs}(t) = 4\pi\sigma D\left(1 + \sigma/\sqrt{\pi Dt}\right), \tag{57}$$

which in the Laplace domain becomes

$$s\hat{k}_{abs}(s) = k_D(1 + \tau(s)), \tag{58}$$

where $\tau(s) \equiv \sigma\sqrt{s/D} = \sqrt{s\tau_m}$ with the molecular time scale $\tau_m = \sigma^2/D$ and $k_D \equiv k_{abs}(t \to \infty) = 4\pi\sigma D$ is the diffusion-limited rate constant for two particles that do not interact except at contact. Substituting this in eqn (54) with $U(\sigma) = 0$ gives

$$\hat{k}_{rad}(s) = \frac{k_a k_D}{s}\frac{1 + \tau(s)}{k_a + k_D(1 + \tau(s))}. \tag{59}$$

This expression yields for the effective association rate $k_{on} = \lim_{s \to 0} s\hat{k}_{rad}(s)$:

$$k_{on} = \frac{k_a k_D}{k_a + k_D}. \tag{60}$$

We note that this expression also follows from the much simpler steady state approximation of the macroscopic rate equations for association, in which the surface σ is viewed as an intermediate state. In this approximation k_a is taken as the rate from the intermediate σ surface to the associated/bound state and k_D is the diffusion limited rate to reach the σ surface from the unbound state. However, the above derivation is more general, and does not require the (rather strong) approximations that are made in the simple approach.

The dissociation rate constant

Following Agmon and Szabo,[1] we will derive the effective dissociation rate constant k_{off} from $S_{rev}(t|*)$:

$$\frac{1}{k_{off}} = \tau_{off} = \int_0^\infty dt[1 - S_{rev}(t|*)]. \tag{61}$$
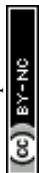
Here $S_{rev}(t|*)$ is the probability that the ligand, which is bound initially, is free at a later time t. The subscript "rev" indicates that during the time t the ligand may bind and unbind many times.

To obtain $S_{rev}(t|*)$, we first consider $S_{rev}(t|r_0)$ and the following boundary condition for eqn (41):[1]

$$4\pi\sigma^2 D \left.\frac{\partial p_{rev}(r,t|r_0)}{\partial r}\right|_{r=\sigma} = k_a p_{rev}(\sigma, t|r_0) - k_d[1 - S_{rev}(t|r_0)]$$
$$= R_{rev}(t|r_0). \tag{62}$$

Using $\hat{R}_{rev}(s|r_0) = 1 - s\hat{S}_{rev}(s|r_0)$ we can rewrite the above boundary condition as

$$\hat{R}_{rev}(s|r_0) = \frac{sk_a}{s + k_d}\hat{p}_{rev}(\sigma, s|r_0). \tag{63}$$

The rate is, analogous to eqn (45),

$$k_{rev}(t) = 4\pi \int dr_0 r_0^2 R_{rev}(t|r_0) p_{eq}(r_0). \tag{64}$$

Using the detailed-balance relation eqn (49), this equation can be combined with eqn (63), to give

$$\hat{k}_{rev}(s) = \frac{sk_a p_{eq}(\sigma)}{s + k_d}\hat{S}_{rev}(s|\sigma). \tag{65}$$

Combining this equation with $\hat{k}_{rev}(s) = \hat{R}_{rev}(s|\sigma)\hat{k}_{abs}(s)$ and $\hat{R}_{rev}(s|\sigma) = 1 - s\hat{S}_{rev}(s|\sigma)$, we can derive that

$$\hat{k}_{rev}(s) = \frac{k_a p_{eq}(\sigma)\hat{k}_{abs}(s)}{k_a p_{eq}(\sigma) + (s + k_d)\hat{k}_{abs}(s)}. \tag{66}$$

We now consider $S_{rev}(t|*)$. Since $S_{rev}(0|*) = 0$, $\hat{R}(s|*) = -s\hat{S}_{rev}(s|*)$. The boundary condition, eqn (62), then becomes

$$\hat{R}_{rev}(s|*) = \frac{sk_a \hat{p}_{rev}(\sigma, s|*) - k_d}{s + k_d}. \tag{67}$$

Exploiting the Laplace transform of the detailed balance condition $k_a p_{rev}(\sigma,t|*) = k_d p_{rev}(*,t|\sigma)$ and the definition $p_{rev}(*,t|\sigma) \equiv 1 - S_{rev}(t|\sigma)$, the above equation yields

$$\hat{S}_{rev}(s|*) = \frac{k_d}{s + k_d}\hat{S}_{rev}(s|\sigma). \tag{68}$$

In the time domain, this gives

$$S_{\text{rev}}(t|*) = k_{\text{d}} \int_0^t \exp\left(-k_{\text{d}}t'\right) S_{\text{rev}}\left(t - t'|\sigma\right) dt'. \tag{69}$$

which can be understood by noting that $k_{\text{d}} \exp(-k_{\text{d}}t')$ is the probability per unit amount of time that the bound ligand dissociates at time t' and $S_{\text{rev}}(t - t'|\sigma)$ is the probability that the dissociated particle, which is now at contact σ, is unbound at a later time $t - t'$ (but it could have associated and dissociated in between multiple times).

Combining eqn (68) with eqn (65) gives

$$\hat{k}_{\text{rev}}(s) = sK_{\text{eq}}\hat{S}_{\text{rev}}(s|*). \tag{70}$$

where $K_{\text{eq}} \equiv k_{\text{a}}p_{\text{eq}}(\sigma)/k_{\text{d}}$. Combining this result with eqn (66), we find

$$s\hat{S}_{\text{rev}}(s|*) = \frac{k_{\text{d}}k_{\text{abs}}(s)}{k_{\text{a}}p_{\text{eq}}(\sigma) + (s + k_{\text{d}})k_{\text{abs}}(s)}. \tag{71}$$

The off rate is then

$$\frac{1}{k_{\text{off}}} = \tau_{\text{off}} = \int_0^\infty dt[1 - S(t|*)] = \lim_{s \to 0}\left[1/s - \hat{S}_{\text{rev}}(s|*)\right] = \frac{1}{k_{\text{d}}} + \frac{K_{\text{eq}}}{k_{\text{D}}}, \tag{72}$$

where, as before, k_{D} is the long-time limit of $k_{\text{abs}}(t)$: $k_{\text{D}} = \lim_{s \to 0} sk_{\text{abs}}(s)$. This result can be rewritten as

$$k_{\text{off}} = \frac{k_{\text{d}}k_{\text{D}}}{k_{\text{a}}p_{\text{eq}}(\sigma) + k_{\text{D}}}, \tag{73}$$

which, using eqn (56), is also given by

$$k_{\text{off}} = k_{\text{d}}S_{\text{rad}}(\infty|\sigma). \tag{74}$$

Indeed, the effective off rate is the intrinsic dissociation rate k_{d} times the probability $S_{\text{rad}}(\infty|\sigma) = k_{\text{D}}/(k_{\text{a}}p_{\text{eq}}(\sigma) + k_{\text{D}})$ that the particle subsequently escapes. As written, the above results for k_{off} hold for any $U(r)$, when $U(r) = 0$ for $r \geq \sigma$, $p_{\text{eq}}(\sigma) = 1$ and $k_{\text{D}} = 4\pi\sigma D$.

Finally, we note that, from eqn (55) and (73), it is clear that the equilibrium constant is also given by

$$K_{\text{eq}} = \frac{k_{\text{a}}p_{\text{eq}}(\sigma)}{k_{\text{d}}} = \frac{k_{\text{on}}}{k_{\text{off}}}. \tag{75}$$

Acknowledgements
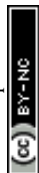
References

1 N. Agmon and A. Szabo, *J. Chem. Phys.*, 1990, **92**, 5270.

2 J. S. van Zon and P. R. ten Wolde, *J. Chem. Phys.*, 2005, **123**, 234910.

3 M. J. Morelli and P. R. ten Wolde, *J. Chem. Phys.*, 2008, **129**, 054112.

4 K. Takahashi, S. Tănase-Nicola and P. R. ten Wolde, *Proc. Natl. Acad. Sci. U. S. A.*, 2010, **107**, 2473–2478.

5 J. Lipková, K. C. Zygalakis, S. J. Chapman and R. Erban, *SIAM J. Appl. Math.*, 2011, **71**, 714–730.

6 M. E. Johnson and G. Hummer, *Phys. Rev. X*, 2014, **4**, 031037.

7 H. C. R. Klein and U. S. Schwarz, *J. Chem. Phys.*, 2014, **140**, 184112.

8 S. H. Northrup and H. P. Erickson, *Proc. Natl. Acad. Sci. U. S. A.*, 1992, **89**, 3338–3342.

9 H.-X. Zhou, *J. Chem. Phys.*, 1998, **108**, 8139.

10 J. S. van Zon, M. J. Morelli, S. Tanase-Nicola and P. R. ten Wolde, *Biophys. J.*, 2006, **91**, 4350.

11 K. Kaizu, W. de Ronde, J. Paijmans, K. Takahashi, F. Tostevin and P. R. ten Wolde, *Biophys. J.*, 2014, **106**, 976–985.

12 I. V. Gopich and A. Szabo, *Proc. Natl. Acad. Sci. U. S. A.*, 2013, **110**, 19784–19789.

13 A. Mugler and P. R. ten Wolde, *Adv. Chem. Phys.*, 2013, **153**, 373–396.

14 A. Mugler, F. Tostevin and P. R. ten Wolde, *Proc. Natl. Acad. Sci. U. S. A.*, 2013, **110**, 5927–5932.

15 T. S. van Erp, D. Moroni and P. G. Bolhuis, *J. Chem. Phys.*, 2003, **118**, 7762.

16 T. S. van Erp and P. G. Bolhuis, *J. Comput. Phys.*, 2005, **205**, 157–181.

17 T. S. van Erp, *Adv. Chem. Phys.*, 2012, **151**, 27–60.

18 R. J. Allen, P. B. Warren and P. R. ten Wolde, *Phys. Rev. Lett.*, 2005, **94**, 018104.

19 R. J. Allen, C. Valeriani and P. Rein ten Wolde, *J. Phys.: Condens. Matter*, 2009, **21**, 463102.

20 M. Von Smoluchowski, *Z. Phys. Chem.*, 1917, **92**, 129.

21 S. H. Northrup, S. A. Allison and J. A. McCammon, *J. Chem. Phys.*, 1984, **80**, 1517.

22 A. Vijaykumar, P. G. Bolhuis and P. R. ten Wolde, *J. Chem. Phys.*, 2015, **143**, 214102.

23 A. Vijaykumar, T. E. Ouldridge, P. R. ten Wolde and P. G. Bolhuis, 2016, to be published.

24 H. C. Berg and E. M. Purcell, *Biophys. J.*, 1977, **20**, 193.

25 W. Bialek and S. Setayeshgar, *Proc. Natl. Acad. Sci. U. S. A.*, 2005, **102**, 10040–10045.

26 P. R. ten Wolde, N. B. Becker, T. E. Ouldridge and A. Mugler, *J. Stat. Phys.*, 2016, **162**, 1395–1424.

27 S. A. Rice, *Diffusion-Limited Reactions*, Elsevier, Amsterdam, 1985.